Materials Research. 2014; 17(6): 1375-1383
DOI: http://dx.doi.org/10.1590/1516-1439.279014

Supramolecular Arrangements of an Organometallic Forming Nanostructured Films

S. A. Camacho[a]*, P. H. B. Aoki[a], F. F. de Assis[b], A. M. Pires[a], K. T. de Oliveira[b],

C. J. L. Constantino[a]

[a]Departamento de Física, Química e Biologia – DFQB, Faculdade de Ciências e Tecnologia, Univ Estadual Paulista – UNESP, CEP 19060-900, Presidente Prudente, SP, Brazil
[b]Departamento de Química, Universidade Federal de São Carlos – UFSCar, Rodovia Washington Luís, km 235 – SP -310, CEP 13565-905, São Carlos, SP, Brazil

Received: March 11, 2014; Revised: July 8, 2014

Organometallic materials have become subject of intensive research on distinct technological applications. The Langmuir-Blodgett (LB) and Langmuir-Schaefer (LS) techniques have proven to be suitable to address challenges inherent to organic devices, in which the film properties can be tuned at molecular level. Here, we report on the supramolecular arrangement of zinc(II)-protoporphyrin(IX) dimethyl ester (ZnPPIX-DME) using the Langmuir, LB and LS techniques, leading to nanostructured films. The π-A isotherms showed that π-π stacking interaction among ZnPPIX-DME molecules takes place at the air/water interface, favoring the formation of Langmuir films closely packed. The controlled growth of the LB and LS films was monitored via UV-Vis absorption spectroscopy, with the thickness per monolayer within 1.3 and 1.7 nm. The homogeneous topography found at microscale is no longer preserved at nanoscale, which is found rougher according to AFM data. The FTIR indicated that the ZnPPIX-DME is isotropically arranged on both LB and LS films.

Keywords: *ZnPPIX-DME, Langmuir film, Langmuir-Blodgett (LB), Langmuir-Schaefer (LS)*

1. Introduction

Porphyrins are a widely investigated class of high conjugated heterocycles[1] in which four pyrrole rings are linked to each other in cyclic form through *meso*-methine bridges. When these molecules contain metals linked to their core structure, they are called metalloporphyrins and form complexes such as heme and chlorophylls[2]. Porphyrins are versatile molecules which physicochemical properties are very sensitive to the modification of their electronic distribution on the pyrrole ring[3]. They have been frequently employed as vapor sensors once their optical spectra can be modified as a result of the interaction between the porphyrin ring and the vapor molecule[4-9]. Specifically, metalloporphyrins have been used as amine vapor sensors due to the specific affinity between the metallic atom and the amine moiety[4]. Other important characteristic of the porphyrins is the ability to transfer oxygen and electrons. This ability comes from their intense Soret and moderate Q bands allowing to collect visible light efficiently in the light-harvesting process[10] and thus make them promising for use in solar energy conversion[10-12] and in light harvesting[13-15].

Most applications involving porphyrins and their derivatives are related to devices such as catalysts[16-18] and sensors[19-24]. Therefore, it is essential the improvement and the development of techniques to obtain porphyrin forming supramolecular structures[25]. In this sense, several kinds of techniques such as micelles[26], vesicles[27], Langmuir-Blodgett (LB) films[28,29], Langmuir-Schaefer (LS) films[3,4] and Layer-by-Layer films[30,31] have been applied and optimized. Among them, LB and LS techniques represent widely employed deposition methods to fabricate porphyrin thin films in a controlled way onto solid substrates[25,32]. The conventional LB and LS techniques allow a supramolecular arrangement that can influence the optical and electrical properties of a deposited film and, as a consequence, the variation of such parameters can be targeted according to desired application to the high-performance devices[32].

In the present study we fabricated and characterized Langmuir film (monolayer at air/ water interface), LB film (Langmuir film vertically transferred from air/water interface onto solid substrate) and LS film (Langmuir film horizontally transferred from air/water interface to solid substrate) of the zinc(II)-protoporphyrin (IX) dimethyl ester (ZnPPIX-DME). Protoporphyrins are a kind of porphyrins that have side chains like methyl, propionic acid and vinyl group[33]. The Langmuir film was studied via surface pressure vs. mean molecular area (π-A) isotherms and was applied such as investigation tool of the π-π stacking interaction. The Brewster Angle Microscopy (BAM) images were also used to the study of the π-A isotherm, allowing visualize at microscopic level, the aggregation state of the molecules in the monolayer. We have also demonstrated the possibility of growing LB and LS multilayer films containing ZnPPIX-DME. The growth of the films was monitored by

*e-mail: sabrina.alessio@gmail.com

ultraviolet-visible absorption (UV-Vis) spectroscopy, while the morphology was investigated by micro-Raman and atomic force microscopy (AFM). The spatial distribution of the LB and LS films with micrometer scale resolution was performed using micro-Raman technique. At nanometer scale, AFM images were characterized via thickness, RMS roughness (RMS, root mean square) and average height (height difference between peaks and valleys). Finally, Fourier transform infrared (FTIR) absorption spectroscopy in reflection and transmission modes was applied to verify a possible anisotropy in terms of molecular organization of ZnPPIX-DME forming LB and LS films.

2. Experimental

2.1. *Material*

The protoporphyrin dimethyl ester (PPIX) was synthesized from hematoporphyrin under acid catalyzed dehydration conditions and also acid catalyzed esterification, which details are described in[34,35]. Thus, the zinc(II)-protoporphyrin (IX) dimethyl ester (ZnPPIX-DME), which molecular structure is given in Figure 1, was prepared from PPIX by simple metalation using $Zn(OAc)_2$ in $CHCl_3$/MeOH. This porphyrinoid was characterized using ^{1}H-NMR and UV-Vis. The dichloromethane (Merck) solvent was HPLC grade. The ultrapure water (18.2 MΩ cm) was acquired from a Milli-Q water purification system (model Simplicity).

2.2. *Langmuir, Langmuir-Blodgett (LB) and Langmuir-Schaefer (LS) films*

The ZnPPIX-DME Langmuir, LB and LS films were fabricated using a Langmuir trough KSV-NIMA model KN 2002. The Langmuir films were produced on water subphase by spreading 40 µL of a 0.50 mg/mL (0.77 mmol/L) ZnPPIX-DME solution dissolved in dichloromethane. The Langmuir monolayers at the air/water interface were characterized by π-A isotherms at 23 °C using the Wilhelmy method with the plate surface placed perpendicular to the barriers. The monolayer was symmetrically compressed under a constant barrier speed at 10 mm/min with the subphase containing ultrapure water. In addition, Brewster angle microscopy (BAM) images were obtained in Langmuir films of ZnPPIX-DME using a KSV micro-BAM microscope. The BAM images were collected for different areas and pressures during the compression of the film at the air/water interface. LB and LS films were obtained by transferring the ZnPPIX-DME Langmuir monolayers from the air/water interface onto different solid substrates depending on the characterization technique to be applied. The surface pressure was kept constant at 30 mN/m and the barrier speed at 10 mm/min (symmetrical compression). LB films were deposited by emerging the substrate vertically with upstroke speeds from 0.2 to 1.0 mm/min. The deeper speed was varied within this interval during the deposition to keep the transfer ratio (TR) close to 1, leading to Z-type LB films. For the LS films, the deposition was carried out approaching manually and horizontally the substrate to the air/water interface.

2.3. *Film characterization*

The ZnPPIX-DME solution in dichloromethane (2.5×10^{-5} mol/L) and the LB and LS film growth were monitored via UV–Vis absorption spectroscopy using a Varian spectrophotometer, model Cary 50, from 190 to 1100 nm. For UV-Vis absorption spectroscopy characterization, LB and LS films containing up to 9 layers were deposited onto quartz substrate. Raman analysis and optical microscopy were carried out using a spectrograph micro-Raman Renishaw model in-Via equipped with a Leica microscope, which 50x objective lens allows collecting the spectra with a spatial resolution of ca. 1 µm^2, a CCD detector, laser lines at 514.5 and 633 nm, 1800 groove/mm gratings

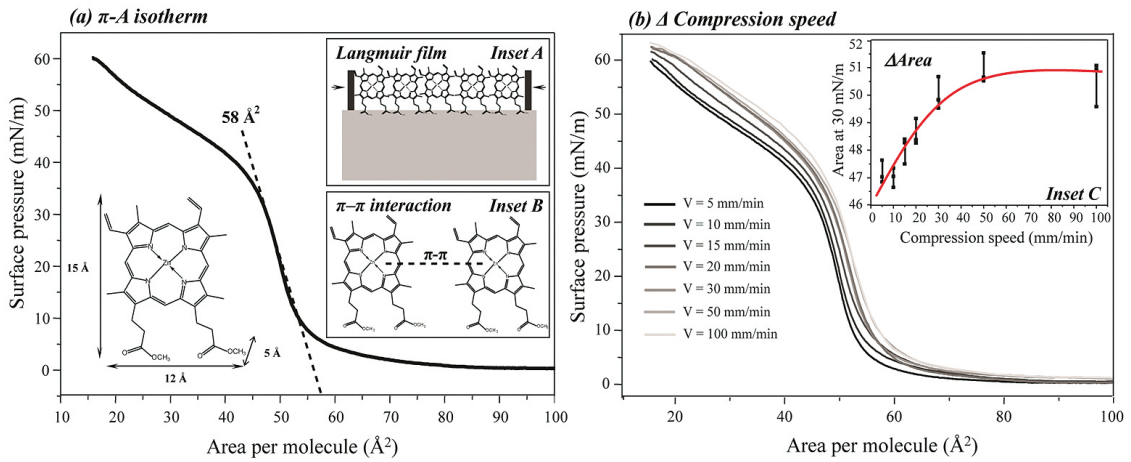

Figure 1. (a) ZnPPIX-DME π-A isotherm recorded for the ultrapure water subphase at room temperature (23 °C). The inset A is a scheme illustrating the ZnPPIX-DME Langmuir film at the air/water interface and inset B the π-π interaction between protoporphyrin rings. The approximate dimension of the ZnPPIX-DME molecule is given as a detail. (b) ZnPPIX-DME π-A isotherms recorded for different compression speeds. The inset C displays the dependence of the corresponding molecular area at 30 mN/m on compression speed (the bars correspond to the interval found for the three isotherms recorded for each compression speed).

with additional edge filters, and a computer-controlled three-axis-encoded (XYZ) motorized stage to take Raman images with a minimum step of 0.1 μm. The AFM images for the LB and LS films were obtained using a Nanosurf instrument model easyScan 2, with a tip of silicon nitride, in the tapping mode. All images were collected with high resolution (512 lines per scan) at a scan rate of 0.5 Hz. The images were characterized by using the software Gwyddion 2.19 to analyze the average height and RMS roughness of the topographic images.

The FTIR measurements were taken using a spectrometer Bruker model Tensor 27 with spectral resolution of 4 cm^{-1} and 128 scans, using a DTGS detector. The spectra in reflection mode were obtained with an incident angle of radiation of 80° using a Bruker accessory A118. LB films with 30 layers were deposited onto Ge substrate and 50 layers on Au mirror for FTIR measurements in transmission and reflection modes, respectively. For LS films 60 layers were deposited onto Ge substrate and Au mirror for the same FTIR measurements.

3. Results and Discussion

3.1. *ZnPPIX-DME Langmuir films*

Figure 1 displays the π-A isotherms of ZnPPIX-DME Langmuir films. The well-defined pattern of the gas, liquid and solid-like phases are not observed during compression of the monolayer. When approaching the solid phase, the π-A isotherm displays high slope toward 35 mN/m. From then on, a phase transition is seen and a long process with a less marked slope takes place. Borovkov et al.[9] and Valli et al.[6] also observed the same phase transition working with Langmuir films of bis(zinc porphyrin) and zinc porphyrin, respectively. Borovkov et al.[9] attributed the existence of these two phases to the increase in size of three-dimensional aggregates. Nevertheless, there are not significant changes in the surface pressure that indicate the monolayer collapse. According to Bergeron et al.[36] the rigidity of such films turns it difficult to determine where exactly the collapse begins.

The occupied area per ZnPPIX-DME molecules is estimated to be ca. 58 $Å^2$ by extrapolating the linear region of the isotherm, before the phase transition, to zero pressure (Figure 1a). Considering the approximate dimensions of the ZnPPIX-DME molecules, the ZnPPIX-DME molecular area into Langmuir films is smaller than the molecular area of the protoporphyrin macrocycle lying flat on the air/water interface (145 $Å^2$). On the other hand, the occupied area (58 $Å^2$) determined via π-A isotherms is comparable to the calculated value (5 × 12 = 60 $Å^2$)[36] for the ZnPPIX-DME with the ester groups facing the air/water interface. A similar molecular arrangement was found by Jin et al.[37] and Li et al.[28] for Langmuir films made of iron(III) and zinc(II) protoporphyrins, respectively. This possible molecular arrangement might be related to a strong attractive π-π interaction between protoporphyrin rings leading to the molecular aggregation at the air/water interface. Indeed, the presence of the ester moieties facing the water subphase favors the formation of Langmuir films closely packed by the strong π-π stacking interaction[28,37], as depicted by insets A and B in Figure 1a.

Figure 1b displays the effect of the compression speed on the packing of the Langmuir film. The dependence of the corresponding molecular area at 30 mN/m on compression speed is shown in inset C. The molecular area increases up to a plateau with the increasing of compression speed. The latter is related to the time the ZnPPIX-DME molecules have to rearrange and pack on the air/water interface. The slower the compression speed the smaller the molecular area due to the formation of Langmuir films closely packed by the strong π-π stacking interaction.

Figure 2a shows different cycles of compression and expansion of ZnPPIX-DME Langmuir films. A small hysteresis is seen after the first cycle, which indicates the formation of molecular aggregates during the first compression. The subsequent cycles reproduce each other indicating that the aggregates formed as a result of the π-π stacking interaction are stable, i.e., they are formed during the first compression and are kept as it is. The BAM images recorded for different compression stages are shown

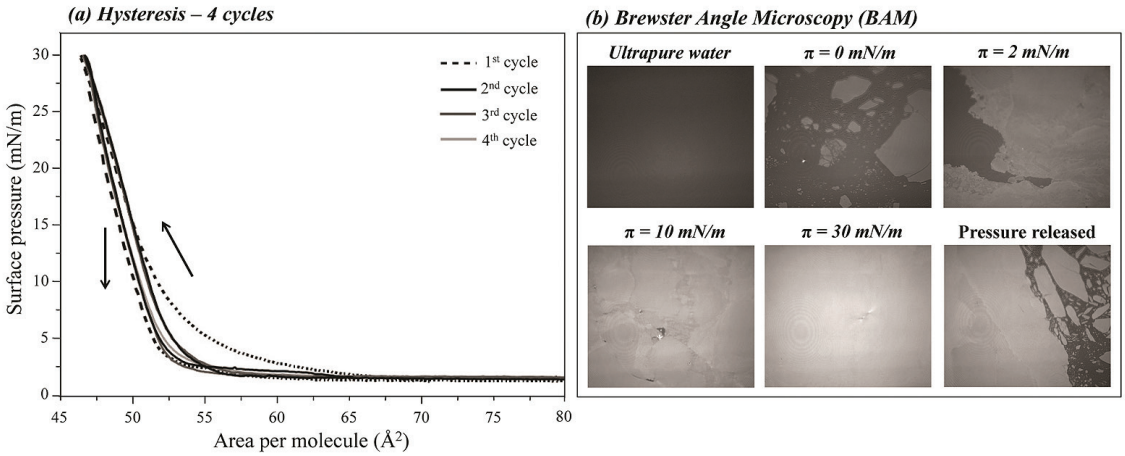

Figure 2. (a) ZnPPIX-DME π-A isotherms obtained by four compression-expansion consecutive cycles. (b) The BAM images recorded for different compression stages of the film.

in Figure 2b. Significant domains are found even before starting the monolayer compression (π = 0 mN/m), which is an evidence of π-π interactions leading to ZnPPIX-DME aggregation. The presence of large domains is still predominant into the gas-phase reached at low surface pressures (π = 2 mN/m) by compressing the monolayer. Borovkov et al.[9] also observed the co-existence of gas and condensed domains in Langmuir films of an bis(zinc porphyrin) and also attributed this event to the presence of aggregates on the water surface. The increase of surface pressure toward the liquid-phase (π = 10 mN/m) and condensed-phase (π = 30 mN/m) increases the Langmuir monolayer uniformity and large domains are no longer observed. This is the stage (named solid phase) in which the Langmuir monolayer is transferred to solid substrates forming either LB or LS films. By releasing the surface pressure of the Langmuir film (expansion), large domains are once more observed, equally to the observed prior compression. The latter is in agreement to the aggregation stability found by the hysteresis in the π-A isotherms.

3.2. *Growth of ZnPPIX-DME forming LB and LS films*

The growth of the LB and LS films was monitored using UV-Vis absorption spectroscopy. Figures 3a and 3b present the UV-Vis spectra for both LB and LS films, respectively, recorded every 2 layers up to 9 layers. The ZnPPIX-DME solution spectrum is given as reference and scaled to fit the plot. The ZnPPIX-DME molecules in the solution exhibit three main absorption bands with maxima at 409, 539 and 577 nm, assigned to one Soret band and two Q-bands[36,38-40], respectively.

The insets in Figures 3a and 3b show the absorbance at 406 and 404 nm for the different numbers of deposited layers in the LB and LS films, respectively. The linear growth of absorbance indicates that similar amounts of ZnPPIX-DME are transferred per deposited monolayer, revealing a controlled growth of both LB and LS films. Besides, in terms of absorbance values, considering that for LB films the monolayers are transferred onto both sides of the substrate while for LS films the monolayers are transferred onto only one side of the substrate, then approximately the same amount of ZnPPIX-DME is deposited per monolayer for both LB and LS films.

3.3. *Morphology at micro and nanometer scales of ZnPPIX-DME forming LB and LS films*

The spatial distribution of the ZnPPIX-DME in the LB and LS films at micrometer scale resolution was performed using micro-Raman technique, combining morphological and chemical information with an optical microscope coupled to a Raman spectrograph. Figures 4a and 4b show the Raman spectra and optical images taken from both ZnPPIX-DME LB and LS films, respectively. Both optical images revealed a highly homogeneous film surface at the microscale, with absence of aggregates. Besides, different spectra recorded from distinct spots present high similarity each other in terms of band frequencies (Figure 4a), indicating that ZnPPIX-DME molecules are homogeneously distributed throughout the LB and LS films.

Slightly differences are found considering the band relative intensities of the spectra collected for LB and LS films. The BAM images (Figure 2b) suggest that Langmuir films are formed by domains that might contain different structuration of ZnPPIX-DME molecules. In micro-Raman experiments, the probed area of the laser is ca. 1μm^2. Therefore, those the differences in Raman spectra might be related to different spots probed by the laser, containing domains with distinct structuration of ZnPPIX-DME molecules. This effect is not comparable to techniques such as FTIR and UV-Vis, which probed area of the radiation beam is about mm^2. The spectra collected in these cases are an average of the combined response of different domains, leading to smaller variation.

Figures 5a and 5b show AFM images (2 and 3 dimensions) for ZnPPIX-DME LB and LS films, respectively. The AFM

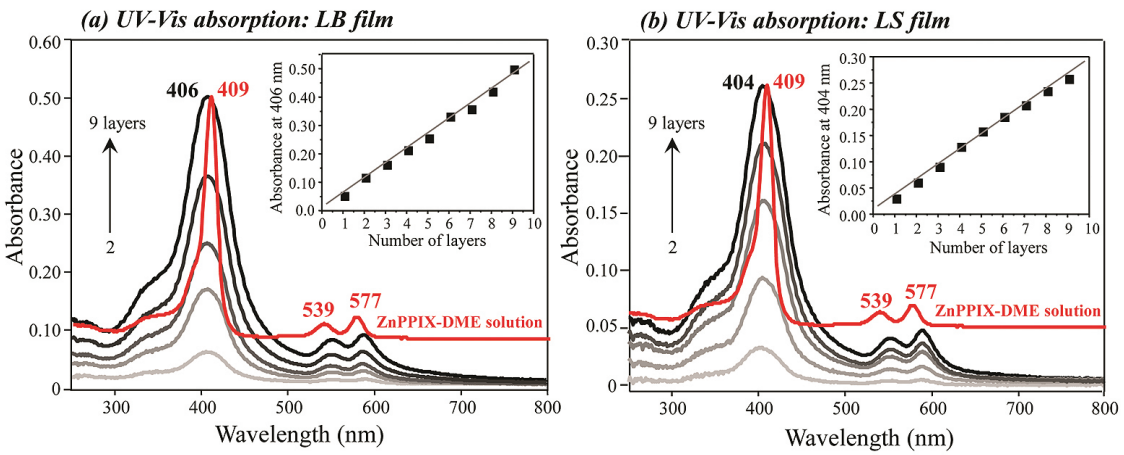

Figure 3. UV-Vis absorption spectra for (a) LB and (b) LS films containing different numbers of ZnPPIX-DME monolayers transferred onto quartz with the ultrapure water subphase at room temperature (23 °C). The films were grown in a constant surface pressure at 30 mN/m. The insets show the absorbance at the Soret band vs. the number of deposited monolayers. The ZnPPIX-DME solution (2.5×10^{-5} mol/L) spectra are given as reference and scaled to fit the plot.

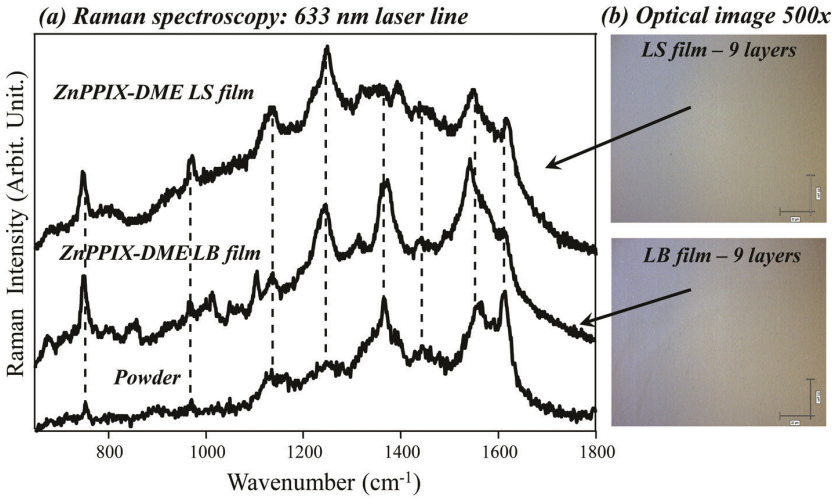

Figure 4. Raman spectra collected for ZnPPIX-DME LB and LS films containing 9 layers each. The spectrum collected for the ZnPPIX-DME powder is given as reference. (b) Optical images recorded for both LB and LS films mentioned in (a). The arrows indicate the spots from where the Raman spectra were recorded.

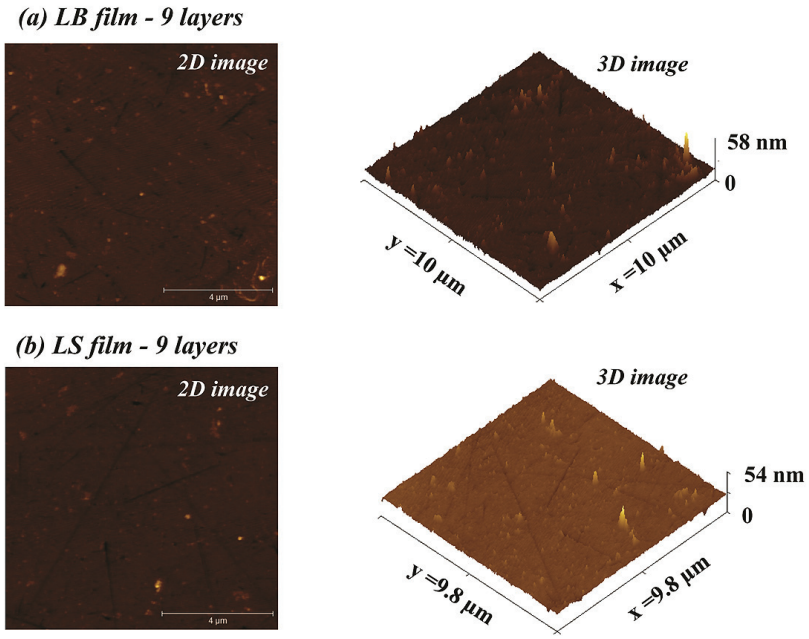

Figure 5. topographic AFM images in 2 and 3 dimensions for 9 layers of ZnPPIX-DME (a) LB and (b) LS films.

images were also characterized via RMS roughness (RMS, root mean square) and average height (height difference between peaks and valleys). The RMS roughness is given by the standard deviation according to the equation $R_{rms} = \sqrt{\frac{\sum_{n=1}^{N}(Z_n - \overline{Z})^2}{N-1}}$ where: $\overline{Z}$ is the average of Z values in the determined area, Zn is the height of the nth pixel, N is the number of pixels considered in the determined area and the average height is simply the arithmetic average of the measured heights. The values of roughness and average height were obtained for areas of 30 µm × 30 µm, 20 µm × 20 µm and 10 µm × 10 µm and are shown in Table 1. The low values in terms of roughness and average height presented by the quartz plate itself (Table 1) ensure greater accuracy for the results obtained for the films.

A visual inspection of the AFM images in Figure 5 reveals the presence of some spikes distributed along the film surfaces (LB and LS), revealing that the homogeneous morphological pattern observed at micrometer scale via micro-Raman is quite different at nanometer scale. Those spikes might be responsible by the relative high values of RMS roughness, average height and the differences found for these values depending on the size of the scanned areas (Table 1). The RMS roughness, for instance, is about 10

to 20% of the thickness of the films (Figure 6). The main difference is the rougher surface displayed by the ZnPPIX-DME LB film compared to the LS one. Li et al.[28] working with neat and mixed LB films of protoporphyrin IX zinc(II) (ZnPP) and surfactants have shown similar features in terms of film topography.

The thickness of the films was also checked by AFM. Figures 6a and 6b show a surface profile produced by scratching both LB and LS films deposited onto Ge plate. The Ge plate was used in this case because its contrast allows one to easier find the film edge. ZnPPIX-DME LB and LS films showed a thickness ranging between 12 and 15 nm considering 9 layers in both cases, which leads to a thickness per layer ranging from 1.3 to 1.7 nm. Considering the dimensions of the ZnPPIX-DME molecules (height = 1.5 nm) and their arrangement at the air/water interface proposed in Figure 1, one can infer that, despite the formation of molecular aggregates, each monolayer forming the LB or LS films has the thickness of one molecule approximately. The equivalent thickness of LB and LS films is in agreement with UV-Vis data, which also demonstrated an equivalent adsorption of materials per layer.

3.4. *Molecular organization of ZnPPIX-DME forming LB and LS films*

Figures 7a and 7b show transmission and reflection FTIR spectra of the ZnPPIX-DME LB and LS films, respectively. The transmission FTIR spectrum of the ZnPPIX-DME powder dispersed in a KBr pellet is given as a reference system for a random molecular orientation.

FTIR measurements in reflection and transmission modes were obtained in order to verify a possible anisotropy in terms of molecular organization of ZnPPIX-DME in the LB and LS films. Specific molecular orientation can be determined by combining FTIR data and surface selection rules[41,42]. Slightly differences are seen when the transmission and reflection spectra of both LB and LS ZnPPIX-DME films are compared. Besides, the spectra recorded for the

Table 1. roughness (RMS) and average height for ZnPPIX-DME LB and LS films.

Sample	Area (μm²)	RMS roughness (nm)	Average height (nm)
	30×30	2.8	1.6
LB film	20×20	2.6	1.6
	10×10	2.3	1.5
	30×30	2.1	1.3
LS film	20×20	1.9	1.3
	10×10	1.4	1.1
	30×30	0.8	1.0
quartz plate	20×20	0.4	0.8
	10×10	0.3	0.7

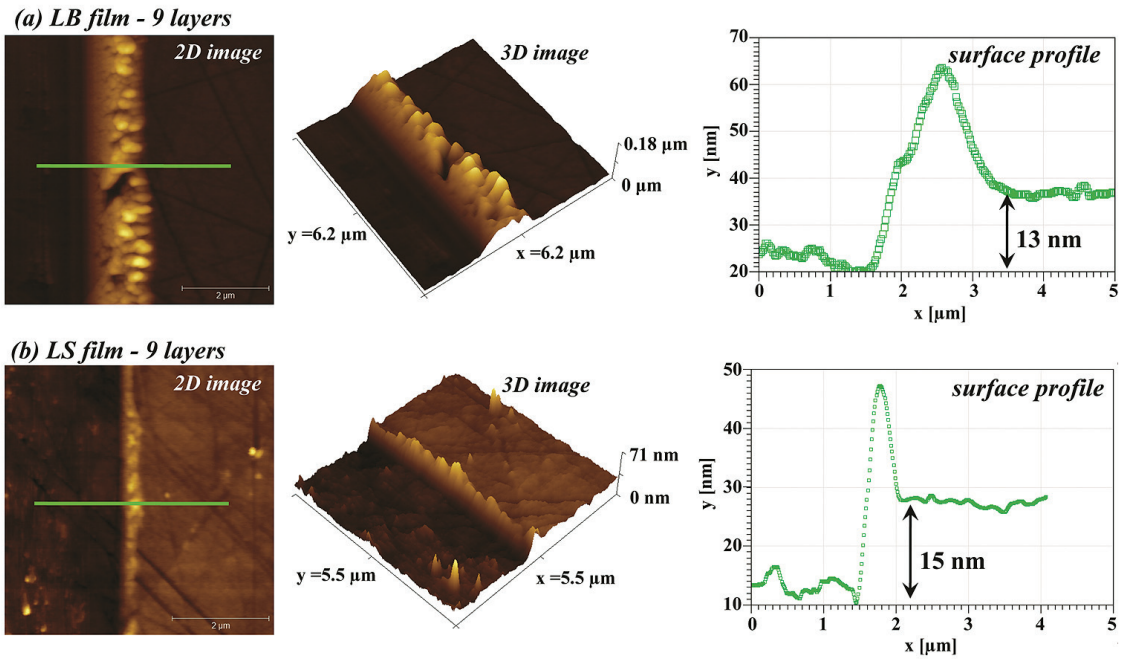

Figure 6. topographic AFM images showing the profiles along an edge for 9 layers of ZnPPIX-DME (a) LB and (b) LS film.

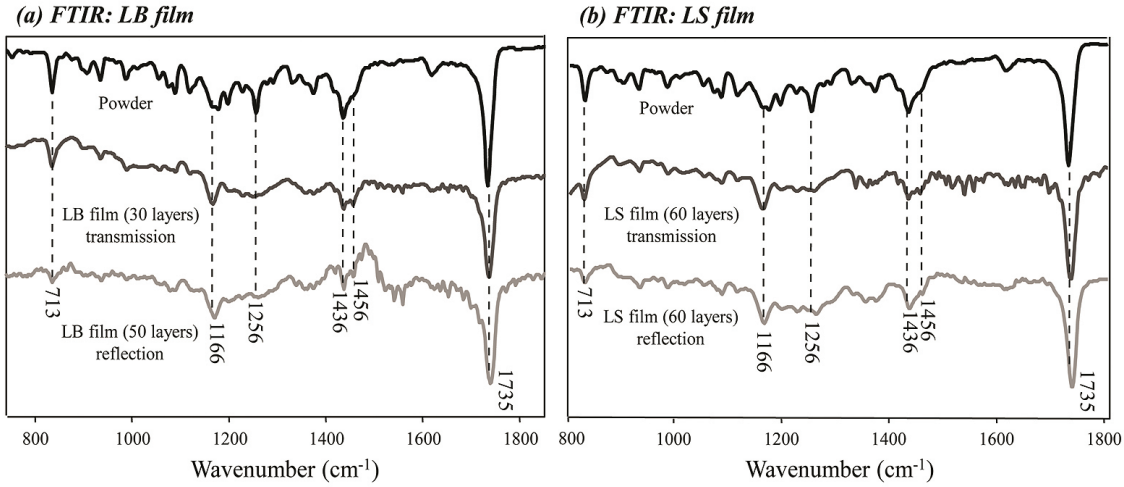

Figure 7. FTIR spectra recorded for the ZnPPIX-DME powder dispersed in KBr pellet and for (a) LB and (b) LS films deposited onto Ge (transmission mode) and onto Au mirror (reflection mode).

films are quite similar to the spectrum of the ZnPPIX-DME powder, suggesting an isotropy of ZnPPIX-DME, *i.e.*, a lack of molecular organization in the films. In a search of the literature we have not found the combination of FTIR measurements, reflection and transmission modes, in order to figure out the anisotropy of LB films of protoporphyrins. Facci et al.[43] have investigated the molecular anisotropy of mesogenic Zn-porphyrin octaesters in LB films by polarized light (Soret band) and infrared (C-H stretching bands) spectroscopy. It was found tilting angles of 40-45° for the macrocycles in the LB layers.

4. Conclusions

The zinc(II)-protoporphyrin (IX) dimethyl ester (ZnPPIX-DME) was successfully applied in the growth of nanostructured films through Langmuir, Langmuir-Blodgett (LB) and Langmuir-Schaefer (LS) techniques, forming supramolecular arrangements. The ZnPPIX-DME molecules are arranged at air/water interface with the ester moieties facing the water subphase, favoring the formation of Langmuir films closely packed by the strong π-π stacking interaction. The LB and LS films were controlled grown onto solid substrates, with an equivalent amount of ZnPPIX-DME molecules per deposited monolayer. The thickness per monolayer for both LB and LS films is coincident with the height of the ZnPPIX-DME molecules, which are homogeneously distributed throughout the films and isotropically arranged in terms of molecular organization. The approach applied here could be extended to other organometallic materials to produce supramolecular arrangements in the form of nanostructured films.

Acknowledgments

This work was supported by the Brazilian agencies FAPESP, CNPq and CAPES.

References

1. Girek B and Sliwa W. Porphyrins functionalized by quaternary pyridinium units. *Journal of Porphyrins and Phthalocyanines*. 2013; 17(12):1139-1156. http://dx.doi.org/10.1142/S1088424613300085
2. Matano Y and Imahori H. Phosphole-containing calixpyrroles, calixphyrins, and porphyrins: synthesis and coordination chemistry. *Accounts of Chemical Research*. 2009; 42(8):1193-1204. PMid:19496532. http://dx.doi.org/10.1021/ar900075e
3. Manera MG, Ferreiro-Vila E, Cebollada A, Garcia-Martin JM, Garcia-Martin A, Giancane G et al. Ethane-bridged zn porphyrins dimers in langmuir-schafer thin films: spectroscopic, morphologic, and magneto-optical surface plasmon resonance characterization. *Journal of Physical Chemistry C*. 2012; 116(19):10734-10742. http://dx.doi.org/10.1021/jp3019843
4. Manera MG, Ferreiro-Vila E, Garcia-Martin JM, Cebollada A, Garcia-Martin A, Giancane G et al. Enhanced magneto-optical SPR platform for amine sensing based on Zn porphyrin dimers. *Sensors and Actuators B-Chemical*. 2013; 182:232-238. http://dx.doi.org/10.1016/j.snb.2013.02.057
5. Tsuda A. Porphyrin nanoclusters for sensoring chemical and physical stimuli. In: Kim D, editor. *Multiporphyrin arrays*: fundamentals and applications. Singapore: Pan Stanford Publishing; 2012. p. 629-660.
6. Valli L, Casilli S, Giotta L, Pignataro B, Conoci S, Borovkov VV et al. Ethane-bridged zinc porphyrin dimers in Langmuir-Shafer thin films: Structural and spectroscopic properties. *Journal of Physical Chemistry B*. 2006; 110(10):4691-4698. PMid:16526704. http://dx.doi.org/10.1021/jp054974v
7. Goletti C, Paolesse R, Di Natale C, Bussetti G, Chiaradia P, Froiio A et al. Optical anisotropy of porphyrin Langmuir-Blodgett films. *Surface Science*. 2002; 501(1-2):31-36. http://dx.doi.org/10.1016/S0039-6028(01)01958-6
8. Latter MJ and Langford SJ. Porphyrinic molecular devices: towards nanoscaled processes. *International Journal of Molecular Sciences*. 2010; 11(4):1878-1887. PMid:20480048 PMCid:PMC2871144. http://dx.doi.org/10.3390/ijms11041878

9. Borovkov VV, Casilli S, Conoci S, Inoue Y, Sortino S and Valli L. Molecular organization and syn reversible arrow anti conformational equilibria in ethane-bridged bis(zinc porphyrin) floating films at the air-water interface. *Surface Science*. 2004; 572(1):66-76. http://dx.doi.org/10.1016/j.susc.2004.08.022
10. Imahori H and Umeyama T. Porphyrin-modified electrodes for solar energy conversion. *Journal of Porphyrins and Phthalocyanines*. 2009; 13(10):1063-1068. http://dx.doi.org/10.1142/S1088424609001315
11. Hasobe T. Porphyrin-based supramolecular nanoarchitectures for solar energy conversion. *Journal of Physical Chemistry Letters*. 2013; 4(11):1771-1780. http://dx.doi.org/10.1021/jz4005152
12. Da Ros T, Prato M, Carano M, Ceroni P, Paolucci F, Roffia S et al. Synthesis, electrochemistry, Langmuir-Blodgett deposition and photophysics of metal-coordinated fullerene-porphyrin dyads. *Journal of Organometallic Chemistry*. 2000; 599(1):62-68. http://dx.doi.org/10.1016/S0022-328X(99)00754-8
13. Kurotobi K, Toude Y, Kawamoto K, Fujimori Y, Ito S, Chabera P et al. Highly asymmetrical porphyrins with enhanced push-pull character for dye-sensitized solar cells. *Chemistry A European Journal*. 2013; 19(50):17075-17081. PMid:24227165. http://dx.doi.org/10.1002/chem.201303460
14. Sprafke JK, Stranks SD, Warner JH, Nicholas RJ and Anderson HL. Noncovalent Binding of Carbon Nanotubes by Porphyrin Oligomers. *Angewandte Chemie International Edition*. 2011; 50(10):2313-2316. PMid:21351343. http://dx.doi.org/10.1002/anie.201007295
15. Wessendorf F, Grimm B, Guldi DM and Hirsch A. Pairing fullerenes and porphyrins: supramolecular wires that exhibit charge transfer activity. *Journal of the American Chemical Society*. 2010; 132(31):10786-10795. PMid:20681711. http://dx.doi.org/10.1021/ja101937w
16. Xiang N, Liu YJ, Zhou WP, Huang H, Guo X, Tan Z et al. Synthesis and characterization of porphyrin-terthiophene and oligothiophene pi-conjugated copolymers for polymer solar cells. *European Polymer Journal*. 2010; 46(5):1084-1092. http://dx.doi.org/10.1016/j.eurpolymj.2010.01.015
17. Lipinska ME, Rebelo SLH and Freire C. Iron(III) porphyrin anchored onto organosilylated multiwalled carbon nanotubes as an active catalyst for epoxidation reactions under mild conditions. *Journal of Materials Science*. 2014; 49(4):1494-1505. http://dx.doi.org/10.1007/s10853-013-7830-7
18. Silva VS, Teixeira LI, Nascimento E, Idemori YM and Defreitas-Silva G. New manganese porphyrin as biomimetic catalyst of cyclohexane oxidation: effect of water or imidazole as additives. *Applied Catalysis A: General*. 2014; 469:124-131. http://dx.doi.org/10.1016/j.apcata.2013.09.033
19. Hamer M, Tomba JP and Rezzano IN. Optical properties and sensor applications of bimetallic nanostructures of porphyrins. *Sensors and Actuators B-Chemical*. 2014; 193:121-127. http://dx.doi.org/10.1016/j.snb.2013.11.077
20. Esteves CHA, Iglesias BA, Li RWC, Ogawa T, Araki K and Gruber J. New composite porphyrin-conductive polymer gas sensors for application in electronic noses. *Sensors and Actuators B-Chemical*. 2014; 193:136-141. http://dx.doi.org/10.1016/j.snb.2013.11.022
21. Paolesse R, Monti D, Nardis S and Natale C D, Porphyrin-based chemical sensors. In: Kadish KM, Smith KM and Guilard R, editors. *Handbook of Porphyrin Science*. Washington: World Scientific Publishing Company; 2011. v. 12, p. 121-225.
22. Tepore A, Serra A, Manno D, Valli L, Micocci G and Arnold DP. Kinetic behavior analysis of porphyrin Langmuir-Blodgett films for conductive gas sensors. *Journal of Applied Physics*. 1998; 84(3):1416-1420. http://dx.doi.org/10.1063/1.368252
23. Richardson TH, Dooling CM, Jones LT and Brook R A. Development and optimization of porphyrin gas sensing LB films. *Advances in Colloid and Interface Science*. 2005; 116(1-3):81-96. PMid:16125660. http://dx.doi.org/10.1016/j.cis.2005.04.009
24. Arnold DP, Manno D, Micocci G, Serra A, Tepore A and Valli L. Gas-sensing properties of porphyrin dimer Langmuir-Blodgett films. *Thin Solid Films*. 1998; 327:341-344. http://dx.doi.org/10.1016/S0040-6090(98)00665-8
25. Hirano C and Imae T. Electrochemical properties of protoporphyrin IX zinc(II) films. *Journal of Colloid and Interface Science*. 2004; 280(2):478-483. PMid:15533420. http://dx.doi.org/10.1016/j.jcis.2004.08.027
26. Jameson LP, Balaz M, Dzyuba SV and Kamiya N. Conformational preference of a porphyrin rotor in confined environments. *RSC Advances*. 2014; 4(2):705-708. http://dx.doi.org/10.1039/c3ra45668d
27. Lin J, Wang SJ, Huang P, Wang Z, Chen SH, Niu G et al. Photosensitizer-Loaded Gold Vesicles with Strong Plasmonic Coupling Effect for Imaging-Guided Photothermal/Photodynamic Therapy. *ACS Nano*. 2013; 7(6):5320-5329. PMid:23721576 PMCid:PMC3709863. http://dx.doi.org/10.1021/nn4011686
28. Li C and Imae T. Protoporphyrin IX zinc(II) organization at the air/water interface and its Langmuir-Blodgett films. *Langmuir*. 2003; 19(3):779-784. http://dx.doi.org/10.1021/la026524p
29. Giancane G and Valli L. State of art in porphyrin Langmuir-Blodgett films as chemical sensors. *Advances in Colloid and Interface Science*. 2012; 171:17-35. PMid:22309985. http://dx.doi.org/10.1016/j.cis.2012.01.001
30. Shen Y, Zhan F, Lu JF, Zhang BY, Huang DK, Xu XB et al. Preparation of hybrid films containing gold nanoparticles and cobalt porphyrin with flexible electrochemical properties. *Thin Solid Films*. 2013; 545:327-331. http://dx.doi.org/10.1016/j.tsf.2013.08.002
31. Krawicz A, Palazzo J, Wang GC and Dinolfo PH. Layer-by-layer assembly of Zn(II) and Ni(II) 5,10,15,20-tetra(4-ethynylphenyl) porphyrin multilayers on Au using copper catalyzed azide-alkyne cycloaddition. *RSC Advances.* 2012; 2(19):7513-7522. http://dx.doi.org/10.1039/c2ra20440a
32. Giancane G, Borovkov V, Inoue Y, Conoci S and Valli L. Syn-anti conformation switching of a bis-porphyrin derivative at the air-water interface and in the solid state as an effective tool for chemical sensing. *Soft Matter.* 2013; 9(7):2302-2307. http://dx.doi.org/10.1039/c2sm27141a
33. Gupta I and Ravikanth M. Recent developments in heteroporphyrins and their analogues. *Coordination Chemistry Reviews*. 2006; 250(3-4):468-518. http://dx.doi.org/10.1016/j.ccr.2005.10.010
34. Adler AD, Longo FR, Kampas F and Kim J. On preparation of metalloporphyrins. *Journal of Inorganic & Nuclear Chemistry*. 1970; 32(7):2443-&. http://dx.doi.org/10.1016/0022-1902(70)80535-8
35. Santos FAB, Uchoa AF, Baptista MS, Iamamoto Y, Serra OA, Brocksom TJ et al. Synthesis of functionalized chlorins sterically-prevented from self-aggregation. *Dyes and Pigments*. 2013; 99(2):402-411. http://dx.doi.org/10.1016/j.dyepig.2013.05.024
36. Bergeron JA, Gaines GL and Bellamy WD. Monolayers of porpyrin esters: spectral disturbances and molecular interactions. *Journal of Colloid and Interface Science*. 1967; 25(1): 97-&. http://dx.doi.org/10.1016/0021-9797(67)90014-8
37. Jin J, Li LS, Wang XQ, Li Y, Zhang YJ, Chen X et al. Steady-state spectroscopic and photovoltage studies of hemin and

hemin/n-octadecylamine Langmuir-Blodgett films. *Langmuir*. 1999; 15(20):6969-6974. http://dx.doi.org/10.1021/la990116c

38. Dolphin D. *The Porphyrins*. New York: Academic Press; 1978.
39. Zhang ZJ and Imae T. Hydrogen-bonding stabilized self-assembled monolayer film of a functionalized diacid, protoporphyrin IX zinc(II), onto a gold surface. *Nano Letters*. 2001; 1(5):241-243. http://dx.doi.org/10.1021/nl000192w
40. Huang XF, Nakanishi K and Berova N. Porphyrins and metalloporphyrins: versatile circular dichroic reporter groups for structural studies. *Chirality*. 2000; 12(4):237-255. http://dx.doi.org/10.1002/(SICI)1520-636X(2000)12:4<237::AID-CHIR10>3.0.CO;2-6
41. Alessio P, Oliveira RF, Aoki PHB, Pereira J, Braunger ML, Furini LN et al. Molecular architecture and electrical properties in evaporated films of cobalt phthalocyanine. *Journal of Nanoscience and Nanotechnology*. 2012; 12(9):7010-7020. PMid:23035427. http://dx.doi.org/10.1166/jnn.2012.6583
42. Debe MK. Optical probes of organic thin-films: photons-in and photons-out. *Progress in Surface Science*. 1987; 24(1-4):1-282. http://dx.doi.org/10.1016/0079-6816(87)90065-7
43. Facci P, Fontana MP, Dalcanale E, Costa M and Sacchelli T. Molecular reorganization in Langmuir-Blodgett films of mesogenic Zn-porphyrin octaesters. *Langmuir*. 2000; 16(20):7726-7730. http://dx.doi.org/10.1021/la000275s